Proceedings of 6th ISJPPE
The 6th International Symposium on Jet Propulsion and Power Engineering
October 16-18, 2017, Beijing, China

2017-ISJPPE-XXXX

Accurate modelling of bearings and seals for rotating machines for power generation

Paolo Pennacchi [a,*], Filippo Cangioli [a], Steven Chatterton [a], Andrea Vania [a]

a. Dept. of Mechanical Engineering, Politecnico di Milano, Via G. La Masa 1, 20156Milan, Italy

Abstract: This paper reviews the most recent achievements obtained in the modelling of oil-film bearings and of labyrinth seals at Politecnico di Milano. These two topics are receiving increasing interest in nowadays rotor dynamics, in particular by OEM, owing to the increasing demand of high-performances/efficiencies and to the remarkable effect that they have on the stability of rotating machinery. The precise evaluation of dynamic coefficients, for both oil-film tilting-pad journal bearings and labyrinth seals, allows reliable evaluation of machine stability in the design phase. At this aim, several models are available in the literature. On the contrary, there are not so many cases, in which the models are validated by means of experimental tests. The bearing and labyrinth seal models presented here are supported by experimental validation.

Keywords: Rotor dynamics; Oil-film bearings; Labyrinth seals; Dynamics stiffness coefficients; Experimental tests

1. Introduction

The current trend in the turbomachinery market is to increase the “flexibility ratio”, which is defined by API standards as the ratio between the steady-state speed and the first critical speed. Because both journal bearings and internal sealing play a pivotal role in the rotordynamic stability, the reliable numerical modelling (i.e. verified with experimental tests) of the dynamic phenomena associated with them deserves much attention.

Tilting pad journal bearings (TPJBs) are widely used in high rotating speed machines mainly due to their high stability compared with plain or fixed-arc journal bearings. Because the dynamic behavior of a rotating machine is strongly influenced by the dynamic characteristics of the bearings, TPJBs have been studied extensively by many authors using numerical simulations and experimental tests. In 1964, Lund [1] introduced his “Lund’s pad assembly method” consisting of calculating the stiffness and damping coefficients for a single fixed non-rotational pad and then summing the contributions from each pad to find the combined effect of the pad assembly.

Over the years, many effective methods have been applied, such as the Newton-Raphson method, numerical analyses, finite elements methods, and genetic algorithms, to calculate the static and dynamic characteristics of journal bearings [2]-[5].

Most of the studies of TPJB in the literature consider load-on-pad (LOP) or load-between-pad (LBP) configurations [6]-[11]. Conversely, studies on the effects of loading direction on the TPJBs are still rare, and most of the papers are limited to theoretical analyses.

Actually, high bearing loads not in the vertical direction may occur in industrial rotating machines, such as in turbo-generators, due to misalignment conditions of the shaft line [12], or in gearboxes. Jones et al. in [13] studied the theoretical effects of load direction on the steady-state and dynamic behavior of tilting pad journal bearings. These authors concluded that a non-symmetrical direction of the load with respect to the pivot positions can produce significant cross-coupling dynamic terms. Additionally, it was found that changing the direction from LOP to LBP tends to reduce the maximum temperature in the bearing, especially when subject to high loads, with negligible effect on power loss.

Moreover, most of the papers in the literature evaluate the static and dynamic characteristics of TPJBs by means of thermo-hydrodynamic (THD) models but assume nominal (i.e. design) dimensions for all bearing pads; that is, the pads have the same nominal geometry, which corresponds to a circular periodicity of the bearing geometry. In practice, the manufacturing tolerances for the pads can be of the same order of magnitude as the oil-film thickness.

This phenomenon is critical for high-speed shafts with a small diameter, where the necessity for large dynamic coefficients is obtained by using small bearing clearances. In the industrial field, the final geometry of the pads is generally tuned by using calibrated shims under the pivots that are able to compensate for the manufacturing tolerances. This solution is not applicable to rocker-backed TPJBs.

Seals are widely used in turbomachinery to reduce the leakage flow through the rotor-stator clearances from the high-pressure to the low-pressure region [14]. The clearance around the rotor is required to avoid rotor-to-stator rub, excessive wear and friction heating. In the case of labyrinth seals, the blades, both for teeth-on-rotor (TOR), teeth-on-stator (TOS) and interlocking configurations, impose a “tortuous passage” to the fluid [15]. The unsteady pressure field produces lateral forces on the shaft that can affect the rotordynamic stability of the machine [16].

The main destabilizing effects are caused by the non-symmetrical unsteady circumferential pressure distribution and by the unbalanced circumferential forces due to the orbit motion of the rotor within the seal.

Regarding the state-of-the-art seal dynamic coefficients estimation, Childs and Scharrer [17] developed a bulk-flow model with a one-control volume (1CV) based on that of Iwatsubo [18] to evaluate the dynamic coefficients of the labyrinth seals composed of a smooth rotor and labyrinth shaped stator (or reverse). Currently, this model is the most used approach in the industrial field to predict seal coefficients. Scharrer [19] has also developed a model with two-control volumes to account for the vortex velocity within the chamber based on the theoretical model of Wyssmann [20].

Nordmann and Weiser [21] developed a bulk-flow model based on three control-volumes for half labyrinth seals. This model considers the continuity, the circumferential momentum and the energy equation in each control-volume; no turbulence model was used because the turbulence effects are taken into account using the wall shear stress correlation reported by Wyssmann [20].

Childs and Scharrer [22] presented the results of the first experimental tests, and Picardo and Childs [23] compared the experimental results of the labyrinth seal coefficients with those estimated using the 1CV bulk-flow model.

The manufacturers of rotating machinery have played a fundamental role in the research on seal effects on the rotordynamic behaviour. A sophisticated test rig equipped with active magnetic bearings was used by Vannini et al. [24]. Some experimental tests were performed for the TOS labyrinth seals with high positive and negative pre-swirl ratios. The test with the negative pre-swirl was performed to investigate the potential impact of swirl reversal devices, such as counter rotating shunt-holes or swirl brakes.

In this paper, the authors introduce an accurate model for TPJB and an improvement in the 1CV bulk-flow model for labyrinth seals, by considering the influence of the energy equation in the zeroth-order solution with real gas properties. The results of both the models developed by the authors are compared to experimental results.

2. Tilting pad journal bearings

The main advantage of a TPJB consists of the pads’ capability to follow the displacements of the rotor. During operation, each pad rotates such that the resultant of the fluid-film forces and the inertial forces due to the mass of the pad passes through the pivot or the contact point between the pad and the bearing ring. Therefore, the pivot location influences the pad rotation and the magnitude of the hydrodynamic pressure distribution.

2.1. TPJB modelling

The bearing model includes the effect of the pad inertia and the pivot stiffness [25], the hydrodynamic lubrication model for the pressure distribution and a simple thermal model for the effect of the temperature distribution on the oil viscosity.

Figure 1 shows in detail the geometry of a single pad from the five shoe rocker-backed TPJB, where O_b and O_j denote the center of the bearing and the journal, respectively.

The pad tilts about the line contact, whose trace is the pivot *P*. Point *P* is also able to moves along the radial direction η due to the flexibility of the pivot. The tangential displacement of the point *P* is neglected. For a given static load, the static equilibrium configuration of the pads (θ_0, η_0) and the corresponding position of the journal center (x_0, y_0) are calculated by using the Newton–Raphson method.

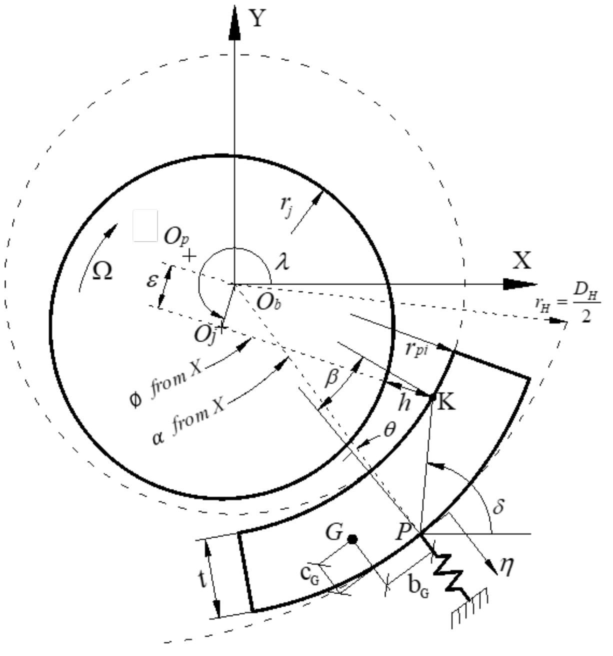

Figure 1 Geometry and coordinate for a single pad.

The first step of modeling the hydrodynamic bearings is the definition of the equation of the oil-film thickness h as a function of the eccentricity and attitude angle, the pad tilt angle and the pad pivoting position.

The pressure distributions of the oil film on each pad are obtained by integrating the Reynolds equation:

$$\begin{aligned}&\frac{\partial}{\partial x}\left(\frac{\rho h^3}{\mu}\frac{\partial p}{\partial x}\right)+\frac{\partial}{\partial z}\left(\frac{\rho h^3}{\mu}\frac{\partial p}{\partial z}\right)=\\&=6\left[\left(U_1-U_2\right)\frac{\partial}{\partial x}\left(\rho h\right)+\rho h\frac{\partial}{\partial x}\left(U_1+U_2\right)+2\rho\left(V_2-V_1\right)\right]\end{aligned} \tag{9}$$

where h is the oil-film thickness, p is the pressure in the fluid film, μ is the lubricant dynamic viscosity, z is the axial direction, x is the tangential direction, and ρ is the density of the oil. The velocity vector components of the shaft and the pads are described by U_1, V_1 and U_2, V_2, respectively

[26].

In particular, the viscosity μ and the density ρ of the lubricating oil are assumed to be functions of only the temperature T :

$$\mu(T)=\mu_{40^\circ C}\exp\left\{\kappa\left(T_{40^\circ C}-T\right)\right\} \tag{10}$$

$$\rho(T)=\rho_{40^\circ C}\left\{1+\alpha_v\left(T_{40^\circ C}-T\right)\right\} \tag{11}$$

where κ and α_v are the viscosity index and the coefficient of thermal expansion of the oil, respectively. In this research, ISO-VG 46 oil was used for bearing lubrication.

The oil film forces in the rotor bearing system can be obtained by:

$$\begin{aligned} f_{x,oil}+W_x&=0\\ f_{y,oil}+W_y&=0 \end{aligned} \tag{12}$$

where $f_{x,oil}$ and $f_{y,oil}$ are the horizontal and vertical hydrodynamic oil-film forces acting on the shaft. W_x and W_y are the resultant forces on the shaft due to the shaft inertia and external load along the horizontal and the vertical direction.

By considering a perturbation Δf_{oil} in the oil-film forces with respect to the static value $f_{oil,0}$ at equilibrium:

$$\begin{aligned} f_{x,oil}&=f_{x,oil,0}+\Delta f_{x,oil}=\sum_k f^k_{x,oil,0}+\sum_k \Delta f^k_{x,oil}\\ f_{y,oil}&=f_{y,oil,0}+\Delta f_{y,oil}=\sum_k f^k_{y,oil,0}+\sum_k \Delta f^k_{y,oil} \end{aligned} \tag{13}$$

the oil-film forces on the shaft are obtained by the sum of the oil-film forces Δf^k_{oil} of each *k*-th pad. The forces $\Delta f^k_{oil}=\Delta f^k_{oil}\left(\Delta x,\Delta y,\Delta\theta,\Delta\eta,\Delta\dot{x},\Delta\dot{y},\Delta\dot{\theta},\Delta\dot{\eta}\right)$ on each pad can be linearized about the equilibrium position by means of the full dynamic coefficients:

$$\begin{aligned} \Delta f^k_{x,oil}&=-k^k_{xx}\Delta x-k^k_{xy}\Delta y-k^k_{x\theta}\Delta\theta-k^k_{x\eta}\Delta\eta-\\ &\quad -c^k_{xx}\Delta\dot{x}-c^k_{xy}\Delta\dot{y}-c^k_{x\theta}\Delta\dot{\theta}-c^k_{x\eta}\Delta\dot{\eta}\\ \Delta f^k_{y,oil}&=-k^k_{yx}\Delta x-k^k_{yy}\Delta y-k^k_{y\theta}\Delta\theta-k^k_{y\eta}\Delta\eta-\\ &\quad -c^k_{yx}\Delta\dot{x}-c^k_{yy}\Delta\dot{y}-c^k_{y\theta}\Delta\dot{\theta}-c^k_{y\eta}\Delta\dot{\eta}\\ \Delta f^k_{\theta,oil}&=-k^k_{\theta x}\Delta x-k^k_{\theta y}\Delta y-k^k_{\theta\theta}\Delta\theta-k^k_{\theta\eta}\Delta\eta-\\ &\quad -c^k_{\theta x}\Delta\dot{x}-c^k_{\theta y}\Delta\dot{y}-c^k_{\theta\theta}\Delta\dot{\theta}-c^k_{\theta\eta}\Delta\dot{\eta}\\ \Delta f^k_{\eta,oil}&=-k^k_{\eta x}\Delta x-k^k_{\eta y}\Delta y-k^k_{\eta\theta}\Delta\theta-k^k_{\eta\eta}\Delta\eta-\\ &\quad -c^k_{\eta x}\Delta\dot{x}-c^k_{\eta y}\Delta\dot{y}-c^k_{\eta\theta}\Delta\dot{\theta}-c^k_{\eta\eta}\Delta\dot{\eta} \end{aligned} \tag{14}$$

where θ and η are the angular rotation and the radial displacement of the *k*-th pad respectively, $\Delta f^k_{\theta,oil}$ and $\Delta f^k_{\eta,oil}$ the moment of the oil-film forces with respect to the pivot and the resultant of the oil-film forces along the radial direction of the pivot position.

By considering a harmonic excitation with a forcing frequency ω, the motion of the system will be:

$$\begin{aligned} \Delta x(t)&=\Delta X(\omega)e^{\mathrm{i}\omega t} & \Delta\dot{X}(\omega)&=\mathrm{i}\,\omega\Delta X(\omega)\\ \Delta y(t)&=\Delta Y(\omega)e^{\mathrm{i}\omega t} & \Delta\dot{Y}(\omega)&=\mathrm{i}\,\omega\Delta Y(\omega)\\ \Delta\theta(t)&=\Delta\Theta(\omega)e^{\mathrm{i}\omega t} & \Delta\dot{\Theta}(\omega)&=\mathrm{i}\,\omega\Delta\Theta(\omega)\\ \Delta\eta(t)&=\Delta\mathrm{N}(\omega)e^{\mathrm{i}\omega t} & \Delta\dot{\mathrm{N}}(\omega)&=\mathrm{i}\,\omega\Delta\mathrm{N}(\omega) \end{aligned} \tag{15}$$

For each pad, the amplitude of oil-film forces in frequency domain can be expressed by:

$$\begin{bmatrix}\Delta F_{x,oil}\\ \Delta F_{y,oil}\\ \Delta F_{\theta,oil}\\ \Delta F_{\eta,oil}\end{bmatrix}^k=-\begin{bmatrix}Z_{xx}&Z_{xy}&Z_{x\theta}&Z_{x\eta}\\ Z_{yx}&Z_{yy}&Z_{y\theta}&Z_{y\eta}\\ Z_{\theta x}&Z_{\theta y}&Z_{\theta\theta}&Z_{\theta\eta}\\ Z_{\eta x}&Z_{\eta y}&Z_{\eta\theta}&Z_{\eta\eta}\end{bmatrix}^k\begin{bmatrix}\Delta X\\ \Delta Y\\ \Delta\Theta_k\\ \Delta\mathrm{N}_k\end{bmatrix} \tag{16}$$

where the matrix of the full dynamic coefficients is given by:

$$\begin{aligned}&\begin{bmatrix}Z_{xx}&Z_{xy}&Z_{x\theta}&Z_{x\eta}\\ Z_{yx}&Z_{yy}&Z_{y\theta}&Z_{y\eta}\\ Z_{\theta x}&Z_{\theta y}&Z_{\theta\theta}&Z_{\theta\eta}\\ Z_{\eta x}&Z_{\eta y}&Z_{\eta\theta}&Z_{\eta\eta}\end{bmatrix}^k=\\ &=\begin{bmatrix}k_{xx}&k_{xy}&k_{x\theta}&k_{x\eta}\\ k_{yx}&k_{yy}&k_{y\theta}&k_{y\eta}\\ k_{\theta x}&k_{\theta y}&k_{\theta\theta}&k_{\theta\eta}\\ k_{\eta x}&k_{\eta y}&k_{\eta\theta}&k_{\eta\eta}\end{bmatrix}^k+\mathrm{i}\,\omega\begin{bmatrix}c_{xx}&c_{xy}&c_{x\theta}&c_{x\eta}\\ c_{yx}&c_{yy}&c_{y\theta}&c_{y\eta}\\ c_{\theta x}&c_{\theta y}&c_{\theta\theta}&c_{\theta\eta}\\ c_{\eta x}&c_{\eta y}&c_{\eta\theta}&c_{\eta\eta}\end{bmatrix}^k\end{aligned} \tag{17}$$

The dynamic coefficients for each pad are obtained using a numerical differentiation approach:

$$\begin{aligned}&[\mathbf{K}]^k=\begin{bmatrix}k_{xx}&k_{xy}&k_{x\theta}&k_{x\eta}\\ k_{yx}&k_{yy}&k_{y\theta}&k_{y\eta}\\ k_{\theta x}&k_{\theta y}&k_{\theta\theta}&k_{\theta\eta}\\ k_{\eta x}&k_{\eta y}&k_{\eta\theta}&k_{\eta\eta}\end{bmatrix}^k=\\ &=\begin{bmatrix}\left.\frac{\partial f_{x,oil}}{\partial x}\right|_0&\left.\frac{\partial f_{x,oil}}{\partial y}\right|_0&\left.\frac{\partial f_{x,oil}}{\partial \theta}\right|_0&\left.\frac{\partial f_{x,oil}}{\partial \eta}\right|_0\\ \left.\frac{\partial f_{y,oil}}{\partial x}\right|_0&\left.\frac{\partial f_{y,oil}}{\partial y}\right|_0&\left.\frac{\partial f_{y,oil}}{\partial \theta}\right|_0&\left.\frac{\partial f_{y,oil}}{\partial \eta}\right|_0\\ \left.\frac{\partial f_{\theta,oil}}{\partial x}\right|_0&\left.\frac{\partial f_{\theta,oil}}{\partial y}\right|_0&\left.\frac{\partial f_{\theta,oil}}{\partial \theta}\right|_0&\left.\frac{\partial f_{\theta,oil}}{\partial \eta}\right|_0\\ \left.\frac{\partial f_{\eta,oil}}{\partial x}\right|_0&\left.\frac{\partial f_{\eta,oil}}{\partial y}\right|_0&\left.\frac{\partial f_{\eta,oil}}{\partial \theta}\right|_0&\left.\frac{\partial f_{\eta,oil}}{\partial \eta}\right|_0\end{bmatrix}^k\end{aligned} \tag{18}$$

$$\begin{aligned}&[\mathbf{C}]^k=\begin{bmatrix}c_{xx}&c_{xy}&c_{x\theta}&c_{x\eta}\\ c_{yx}&c_{yy}&c_{y\theta}&c_{y\eta}\\ c_{\theta x}&c_{\theta y}&c_{\theta\theta}&c_{\theta\eta}\\ c_{\eta x}&c_{\eta y}&c_{\eta\theta}&c_{\eta\eta}\end{bmatrix}^k=\\ &=\begin{bmatrix}\left.\frac{\partial f_{x,oil}}{\partial \dot{x}}\right|_0&\left.\frac{\partial f_{x,oil}}{\partial \dot{y}}\right|_0&\left.\frac{\partial f_{x,oil}}{\partial \dot{\theta}}\right|_0&\left.\frac{\partial f_{x,oil}}{\partial \dot{\eta}}\right|_0\\ \left.\frac{\partial f_{y,oil}}{\partial \dot{x}}\right|_0&\left.\frac{\partial f_{y,oil}}{\partial \dot{y}}\right|_0&\left.\frac{\partial f_{y,oil}}{\partial \dot{\theta}}\right|_0&\left.\frac{\partial f_{y,oil}}{\partial \dot{\eta}}\right|_0\\ \left.\frac{\partial f_{\theta,oil}}{\partial \dot{x}}\right|_0&\left.\frac{\partial f_{\theta,oil}}{\partial \dot{y}}\right|_0&\left.\frac{\partial f_{\theta,oil}}{\partial \dot{\theta}}\right|_0&\left.\frac{\partial f_{\theta,oil}}{\partial \dot{\eta}}\right|_0\\ \left.\frac{\partial f_{\eta,oil}}{\partial \dot{x}}\right|_0&\left.\frac{\partial f_{\eta,oil}}{\partial \dot{y}}\right|_0&\left.\frac{\partial f_{\eta,oil}}{\partial \dot{\theta}}\right|_0&\left.\frac{\partial f_{\eta,oil}}{\partial \dot{\eta}}\right|_0\end{bmatrix}^k\end{aligned} \tag{19}$$

where $[\mathbf{K}]^k$ and $[\mathbf{C}]^k$ are the linear stiffness and damping coefficient matrices; $(x_0,y_0,\theta_0,\eta_0,0,0,0,0)$ represents the static equilibrium position of the system (shaft and pads).

Equation (16) can be rewritten as:

$$\begin{bmatrix}\Delta F_{x,oil}\\ \Delta F_{y,oil}\end{bmatrix}^k = -\begin{bmatrix}Z_{xx} & Z_{xy}\\ Z_{yx} & Z_{yy}\end{bmatrix}^k \begin{bmatrix}\Delta X\\ \Delta Y\end{bmatrix} - \begin{bmatrix}Z_{x\theta} & Z_{x\eta}\\ Z_{y\theta} & Z_{y\eta}\end{bmatrix}^k \begin{bmatrix}\Delta \Theta\\ \Delta \mathrm{N}\end{bmatrix}^k$$
$$\begin{bmatrix}\Delta F_{\theta,oil}\\ \Delta F_{\eta,oil}\end{bmatrix}^k = -\begin{bmatrix}Z_{\theta x} & Z_{\theta y}\\ Z_{\eta x} & Z_{\eta y}\end{bmatrix}^k \begin{bmatrix}\Delta X\\ \Delta Y\end{bmatrix} - \begin{bmatrix}Z_{\theta\theta} & Z_{\theta\eta}\\ Z_{\eta\theta} & Z_{\eta\eta}\end{bmatrix}^k \begin{bmatrix}\Delta \Theta\\ \Delta \mathrm{N}\end{bmatrix}^k \quad (20)$$

From the equation of motion of each pad, amplitudes of vibration along θ and η are given by:

$$\begin{bmatrix}\Delta \Theta\\ \Delta \mathrm{N}\end{bmatrix}^k = \left(-\omega^2\left[M_{pad}\right]^k + \mathrm{i}\omega\left[C_{pad}\right]^k + \left[K_{pad}\right]^k\right)^{-1} \begin{bmatrix}\Delta F_{\theta,oil}\\ \Delta F_{\eta,oil}\end{bmatrix}^k \quad (21)$$

where $\left[M_{pad}\right]^k$, $\left[C_{pad}\right]^k$ and $\left[K_{pad}\right]^k$ are the mass, the damping and the stiffness matrices of the pad, representing the inertia, the damping and stiffness of the pivot respectively:

$$\left[M_{pad}\right]^k = \begin{bmatrix}J_P & m\,b_G\\ m\,b_G & m\end{bmatrix}^k$$
$$\left[C_{pad}\right]^k = \begin{bmatrix}c_\theta & 0\\ 0 & c_\eta\end{bmatrix}^k \quad (22)$$
$$\left[K_{pad}\right]^k = \begin{bmatrix}k_\theta & 0\\ 0 & k_\eta\end{bmatrix}^k$$

where J_P is the mass moment of inertia of the pad with respect to pivot point *P*, m the mass and b_G the position of the barycenter with respect to the pivot. The parameters c_θ, c_η and k_θ have been neglected and only the pivot stiffness k_η has been considered in the evaluation of the dynamic coefficients.

The stiffness of the pivot along the direction η is obtained by the contact Hertz theory as [28]:

$$k_\eta = \frac{\pi E L}{2\left(1-\nu^2\right)\left[\dfrac{2}{3} + \ln\dfrac{8EL\left(r_H - r_{pe}\right)}{2.15^2 F_{P0}}\right]} \quad (23)$$

where E and ν are the Young's modulus and the Poisson coefficient respectively, r_H and r_{pe} are the radii of the bearing housing and pivot and F_{P0} is the load along the radial direction of the pivot. Therefore from Eqs. (20) and (21):

$$\begin{bmatrix}\Delta \Theta\\ \Delta \mathrm{N}\end{bmatrix}^k =$$
$$= -\left(\begin{bmatrix}Z_{\theta\theta} & Z_{\theta\eta}\\ Z_{\eta\theta} & Z_{\eta\eta}\end{bmatrix}^k - \omega^2\left[M_{pad}\right]^k + \mathrm{i}\omega\left[C_{pad}\right]^k + \left[K_{pad}\right]^k\right)^{-1} \quad (24)$$
$$\begin{bmatrix}Z_{\theta x} & Z_{\theta y}\\ Z_{\eta y} & Z_{\eta y}\end{bmatrix}^k \begin{bmatrix}\Delta X\\ \Delta Y\end{bmatrix}$$

From Eq. (13) in the frequency domain, it is possible to obtain the reduced set of dynamic coefficients $\left[\mathbf{Z}\right] = \left[\mathbf{K}\right] + \mathrm{i}\omega\left[\mathbf{C}\right]$:

$$\begin{bmatrix}\Delta F_{x,oil}\\ \Delta F_{y,oil}\end{bmatrix} = -\begin{bmatrix}\sum_k \Delta F^k_{x,oil}\\ \sum_k \Delta F^k_{y,oil}\end{bmatrix} =$$
$$= -\sum_k\left(-\begin{bmatrix}Z_{xx} & Z_{xy}\\ Z_{yx} & Z_{yy}\end{bmatrix}^k \begin{bmatrix}\Delta X\\ \Delta Y\end{bmatrix} - \begin{bmatrix}Z_{x\theta} & Z_{x\eta}\\ Z_{y\theta} & Z_{y\eta}\end{bmatrix}^k \begin{bmatrix}\Delta \Theta\\ \Delta \mathrm{N}\end{bmatrix}^k\right) =$$
$$= \sum_k \left(\begin{gathered}\begin{bmatrix}Z_{xx} & Z_{xy}\\ Z_{yx} & Z_{yy}\end{bmatrix}^k - \begin{bmatrix}Z_{x\theta} & Z_{x\eta}\\ Z_{y\theta} & Z_{y\eta}\end{bmatrix}^k \\ \left(\begin{bmatrix}Z_{\theta\theta} & Z_{\theta\eta}\\ Z_{\eta\theta} & Z_{\eta\eta}\end{bmatrix}^k - \omega^2\left[M_{pad}\right]^k + \mathrm{i}\omega\left[C_{pad}\right]^k + \left[K_{pad}\right]^k\right)^{-1} \\ \begin{bmatrix}Z_{\theta x} & Z_{\theta y}\\ Z_{\eta y} & Z_{\eta y}\end{bmatrix}^k\end{gathered}\right) \begin{bmatrix}\Delta X\\ \Delta Y\end{bmatrix} = \quad (25)$$
$$= -\begin{bmatrix}Z_{xx} & Z_{xy}\\ Z_{yx} & Z_{yy}\end{bmatrix} \begin{bmatrix}\Delta X\\ \Delta Y\end{bmatrix} = -\left[\mathbf{Z}\right]\begin{bmatrix}\Delta X\\ \Delta Y\end{bmatrix}$$

In the literature, the dynamic coefficients are evaluated by considering the load acting in the opposite direction of the Y axis (Figure 2 (a)). If the direction of the load changes, it is still possible to evaluate the dynamic coefficients in the reference system of the load where the Y' axis is aligned in the opposite direction of the load (Figure 2 (b)) by means of the following transformations:

$$\left[\mathbf{K}'\right] = \left[\mathbf{R}\right]^T\left[\mathbf{K}\right]\left[\mathbf{R}\right] \quad (26)$$

$$\left[\mathbf{C}'\right] = \left[\mathbf{R}\right]^T\left[\mathbf{C}\right]\left[\mathbf{R}\right] \quad (27)$$

where $\left[\mathbf{R}\right]$ is a rotation matrix

$$\left[\mathbf{R}\right] = \begin{bmatrix}\cos\beta & -\sin\beta\\ \sin\beta & \cos\beta\end{bmatrix} \quad (28)$$

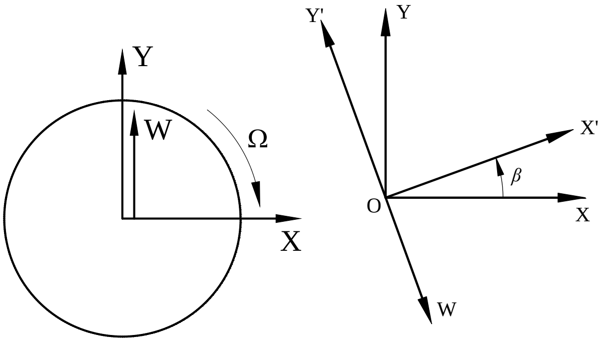

(a) (b)

Figure 2 Direction of the load with respect to the reference system.

A finite-difference code has been developed for the integration of the Reynolds equation. For instance, the pressure $p_{i,j}$ at node (i, j) of the mesh grid is given by a combination of pressures of the nearest nodes:

$$p_{i,j} = a_0 + a_1\, p_{i+1,j} + a_2 p_{i-1,j} + a_3 p_{i,j+1} + a_4 p_{i,j-1} \quad (29)$$

A simple two-dimensional control-volume thermal model [27] is considered for the evaluation of the bearing fluid temperatures and viscosities. A constant average temperature of the oil in the radial direction (y) and adiabatic conditions at the pad and shaft surfaces are considered. A more realistic isothermal condition for the shaft can be obtained using a more sophisticated but time-consuming three-dimensional model. For instance, the temperature T_P of the center (Pole) of each control volume (which is a quadrilateral with dimensions ΔX and ΔZ) is given by a combination of the temperatures T_N, T_E, T_S, T_W of the four edges (North, East, South, West) of the control volume and the temperature of the preceding iteration cycle T_{P0}:

$$T_P = \frac{a_E T_E + a_W T_W + a_S T_S + a_N T_N + S_C \Delta X \Delta Z + \lambda T_{P0}}{a_E + a_W + a_S + a_N - S_P \Delta X \Delta Z + \lambda} \tag{30}$$

The parameter λ is used to enforce the flow directionality (convention) in Eq. (30) depending on the difference between the lubricant flow *in* and *out* of the control volume:

$$\begin{aligned} &\lambda_1 = |a_E| + |a_W| + |a_S| + |a_N| - |a_P| \\ &\lambda = \lambda_1 \quad \text{if} \quad \lambda_1 > 0 \\ &\lambda = 0 \quad \text{if} \quad \lambda_1 \le 0 \end{aligned} \tag{31}$$

where

$$\begin{aligned} a_W &= \frac{h_W \Delta X}{2}\left(\rho_W W_W cp_W + \rho_P W_P cp_P\right) \\ a_E &= -\frac{h_E \Delta X}{2}\left(\rho_E W_E cp_E + \rho_P W_P cp_P\right) \\ a_N &= -\frac{h_N \Delta Z}{2}\left(\rho_N U_N cp_N + \rho_P U_P cp_P\right) \\ a_S &= \frac{h_S \Delta Z}{2}\left(\rho_S U_S cp_S + \rho_P U_P cp_P\right) \end{aligned} \tag{32}$$

In the Eq. (30), the terms S_C and S_P are obtained from the intensity of the viscous heating S by assuming a linear dependence of the heat source term on the temperature:

$$\begin{aligned} S &= \mu_0 \left[\left(\frac{\partial u}{\partial y}\right)^2 + \left(\frac{\partial w}{\partial y}\right)^2\right] h_P = S_c + S_p T_P \\ S_P &= \frac{S}{\mu_0}\frac{d\mu}{dT} \\ S_C &= S\left(1 - \frac{T_{P0}}{\mu_0}\frac{d\mu}{dT}\right); \end{aligned} \tag{33}$$

where the terms μ_0 and T_{P0} refer to the previous sweep of the iteration for temperature.

In this paper, the temperature of the inlet oil used for the numerical model was maintained at 40°C, which corresponds to the actual operating condition of the bearing.

In conclusion, for a given static load, the following conditions must be satisfied:

- convergence of the pressure distribution in each pad;
- convergence of the temperature distribution in each pad;
- equilibrium of the forces on each pad;
- equilibrium of the forces on the shaft for the given static load.

2.2. TPJB experimental tests and results

The test rig of the Dept. of Mechanical Engineering of Politecnico di Milano, is described in detail in [29] and shown in Figure 3.

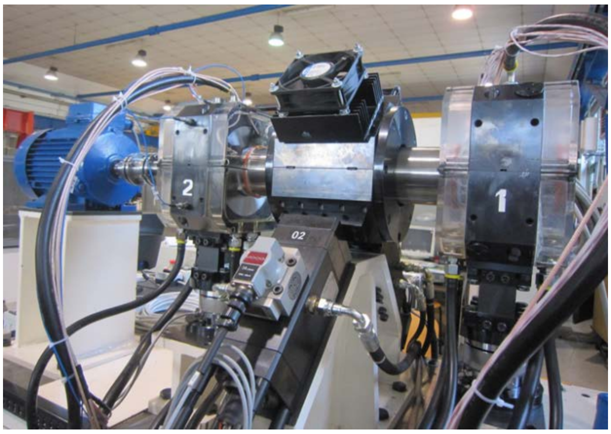

Figure 3 Test rig for journal bearings.

In the test rig, the rotor axis describes orbits similar to the real configuration of a rotating machine thanks to the hydraulic actuators. Moreover, the hydraulic actuators can also apply the static load in any direction of the vertical plane. The static behavior and the dynamic coefficients are evaluated on the bearing #1 in Figure 4, while bearing #2 has the same loads and nominal dimensions.

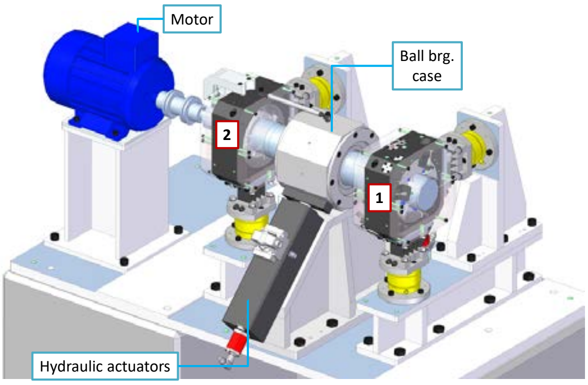

Figure 4 Sketch of the test rig.

Before starting the experimental tests, the actual geometry of the TPJB #1, and the actual preloads of all the pads has been determined by means of the procedure described in [29]. Instead of the standard least square method used in the literature (see for instance [30]) foe estimating the dynamic coefficients, a more robust M-estimator based method has been used, as described in [29] and [31].

2.2.1. Shaft center locus

For the nominal bearing, the numerical journal locus obtained by changing the direction of the static load is a “smoothed pentagon”, which can be approximated by a circle with a radius of approximately 30 µm, as shown in Figure 5 (solid black line with dot markers).

Figure 5 shows the nominal (black dashed-dotted line) and measured (green solid line) pentagonal clearance profile of the nominal and actual TPJBs, respectively. The calculated and measured shaft center locus for the bearing under test and the nominal bearing are plotted inside the measured clearance profile. Twenty positions of the shaft center have been measured, corresponding to twenty directions of the static load (from –90° to 252°, with steps of 18°). For the test bearing, the journal center loci (the calculated one and the measured one) have irregular shapes.

It should be noted that, although there is a difference between prediction and measurement of the journal center locus, their irregular shapes are similar. This fact is probably due to the flexibility of the system and the thermal expansion of the bearing housing during the experiments. During the experimental tests, while the temperature of the oil input is maintained at approximately 40±1°C using a heat exchanger and a temperature controller, the temperature of the housing is greater and is approximately equal to 48°C. This causes an expansion of the mechanical components of the bearing.

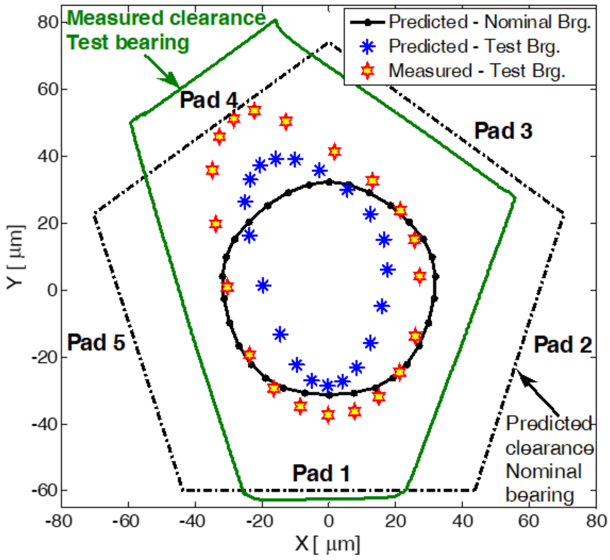

Figure 5 Shaft center locus of the bearing vs. static load direction.

The overall system flexibility include backlashes and stiffness of the system from the pivot to the proximity probe position. These two factors have not been modelled in the mathematical model. The simple thermal model for the oil-film temperature distribution affects the oil-film thickness and pressure distribution. The pivot stiffness considers only the deformation due to the contact between the pad and the bearing housing. The effect of the thermal expansion and system flexibility is a static radial offset in the measurement of the static position of the shaft. Improvement in the model can be obtained by including the additional flexibility of the system in the pivot stiffness given in Eq. (23).

It is interesting to observe that the clearance profile of the test bearing, shown in Figure 5, is greater in the case of pad #4. This effect is likely a consequence of the fact that pad #4 has the smallest thickness (15.981 mm vs. the nominal 16.000 mm), so the displacement of the shaft will be greater in the case of pad #4.

2.2.2. Dynamic coefficients

In the absolute reference system, the vertical load direction is considered varying and the static load is rotated in a full revolution (360°) in steps of 18°. This means that all five pads will be loaded under a LOP and LBP configuration during the tests.

Figure 6 shows the influence of the load direction on the experimental and calculated stiffness and damping coefficients of the test bearing. Obviously, the load direction has a strong effect on both of them.

The stiffness coefficients of the test bearing show a general good agreement between the experimental and the calculated values. The differences can be explained, as previously mentioned, by the fact that the measured displacements of the shaft are greater than the calculated ones due to the thermal expansion and flexibility of the housing-pivot system. Consequently, the calculated direct stiffness coefficients are greater than the experimental coefficients. However, this difference is not noteworthy except for the direct stiffness in the horizontal direction (k_{xx}).

The damping coefficients obtained from the experimental tests are rather different from the calculated coefficients; in particular, the calculated direct coefficients (c_{xx} and c_{yy}) are greater than the experimental coefficients. It is also possible to observe in Figure 6 that the calculated stiffness and damping coefficients of the nominal bearing maintain a certain symmetry as a function of the direction of the load. This is less evident for the test bearing due to the asymmetric geometry.

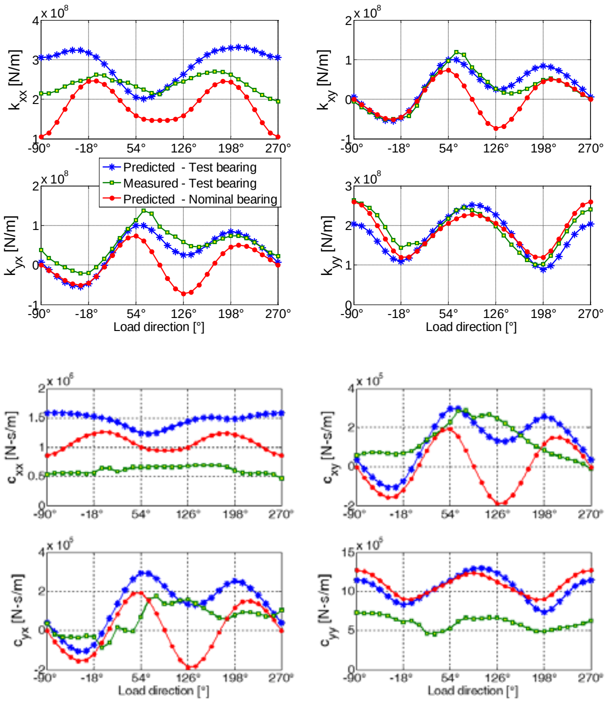

Figure 6 Dynamic coefficients vs. load directions in the absolute reference system.

3. Labyrinth seals

The influence of the seals on the system stability can be predicted using the dynamic coefficients. The prediction of the seal coefficients is challenging because errors in the prediction of the dynamic behaviour may result in dangerous and costly consequences. The effective damping [14] due to sealing components is defined as:

$$c_{eff} = c_{xx} - \frac{k_{xy}}{\omega} \tag{34}$$

and is a key characteristic that should be predicted accurately to investigate the stability of the machine. The effective stiffness is defined as:

$$k_{eff} = k_{xx} - c_{xy}\omega \tag{35}$$

and is relevant to the rotor natural frequency. This is usually not relevant for rotordynamic design when labyrinth seals are considered because it is at least one order of magnitude lower than the journal bearing effective stiffness.

3.1. Model for the calculation of seal dynamic coefficients

The proposed model is based on the 1CV bulk-flow model introduced by Childs and Scharrer [17]. One control volume for each cavity is considered (see Figure 7 and Figure 8).

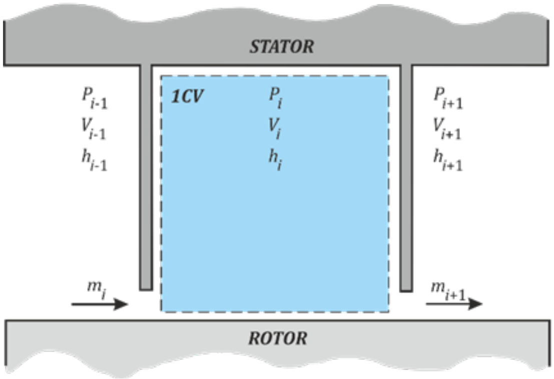

Figure 7 Seal cavity: indices of control variables.

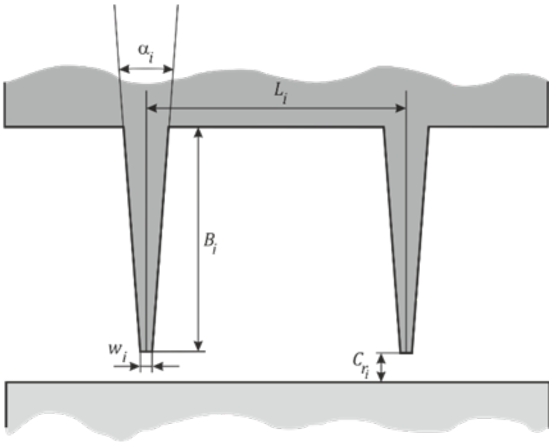

Figure 8 Seal cavity: domain geometry parameters.

The model includes real gas properties evaluated using the NIST code [32] since the ideal gas law could be not verified for severe operating conditions and for several working fluids. The perturbation analysis is used to solve the partial differential equations that govern the phenomena. The rotor position is perturbed with respect to the centred position (see Figure 9), and a circular orbit is assumed, which was suggested by Thorat and Childs [33], to avoid possible inaccuracies due to the frequency-dependent coefficients.

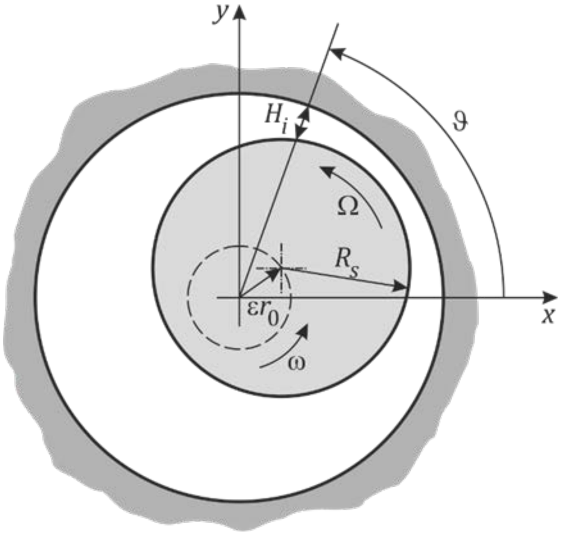

Figure 9 Circular orbit of the centre of the rotor due to the perturbation.

Whilst the models introduced in [17] and [33] considers an isenthalpic process for the fluid within the seal, the model developed by the authors considers the energy balance within each cavity of the seal. Moreover, the authors assume that the perturbed motion of the rotor does not affect the enthalpy in the cavity; hence, the energy equation is evaluated only in the zeroth-order solution (centred rotor).

For an ideal labyrinth seal with no rotating shaft, the enthalpy of the fluid within the seal should be conserved assuming there is no heat exchange between the fluid and the wall boundaries. However, an enthalpy variation along the seal is expected and is caused by the residual kinetic energy of the fluid within each cavity of the seal. The leakage correlation takes into account the variation in the kinetic energy, which is related to the axial velocity, using the kinetic carry-over coefficient. The authors assumed that the main variation in the kinetic energy along the seal, in steady-state condition, is due to the circumferential velocity component; in fact, the energy equations do not consider the axial velocity terms in the zeroth-order solution.

Actually, an isenthalpic process does not represent a correct physic assumption for the description of the fluid-structure interaction within the seal, at least when the rotor is running at a high rotational speed (work performed by the fluid is introduced in the energy equation).

The thermodynamic and kinematic variables of the model are separated in the steady-state terms (index $_{0i}$) and in the perturbed terms (index $_{1i}$).

$$P_i = P_{0i} + \varepsilon P_{1i}(t, \vartheta) \tag{36}$$

$$\rho_i = \rho_{0i} + \varepsilon \rho_{1i}(t, \vartheta) \tag{37}$$

$$h_i = h_{0i} \tag{38}$$

$$V_i = V_{0i} + \varepsilon V_{1i}(t, \vartheta) \tag{39}$$

$$H_i = C_{ri} + \varepsilon H_1(t, \vartheta) \tag{40}$$

The zeroth-order solution of the partially derivative equations, introduced thereafter, addresses the steady-state problem, which is critical for the solutions of the first-order equations that rule the stability of the system.

The physics of the problem is governed by the continuity, circumferential momentum and energy equation (adiabatic process), which are, respectively:

- Continuity equation [17]:

$$\frac{\partial}{\partial t}(\rho_i A_i) + \frac{\partial}{\partial \vartheta}\left(\frac{\rho_i A_i V_i}{R_S}\right) + \dot{m}_{i+1} - \dot{m}_i = 0 \tag{41}$$

- Circumferential momentum equation [17]:

$$\begin{gathered} \frac{\partial}{\partial t}(\rho_i A_i V_i) + \frac{\partial}{\partial \vartheta}\left(\frac{\rho_i A_i V_i^2}{R_S}\right) + \dot{m}_{i+1} V_1 - \dot{m}_i V_{i-1} = \\ = -\frac{A_i}{R}\frac{\partial P_i}{\partial \vartheta} + \tau_{ri} a_{ri} L_i - \tau_{si} a_{si} L_i \end{gathered} \tag{42}$$

- Energy equation [34]:

$$\begin{gathered} \frac{\partial}{\partial t}\left(\left(u_i + \frac{V_i^2}{2}\right)\rho_i A_i\right) + \frac{\partial}{\partial \vartheta}\left(\left(h_i + \frac{V_i^2}{2}\right)\frac{\rho_i A_i V_i}{R_s}\right) + \\ + \dot{m}_{i+1}\left(h_i + \frac{V_i^2}{2}\right) - \dot{m}_i\left(h_{i-1} + \frac{V_{i-1}^2}{2}\right) = \tau_{ri} a_{ri} L_i R_s \Omega \end{gathered} \tag{43}$$

The leakage correlation employed in the model is the generalized Neumann equation for real gases:

$$\dot{m}_i = \mu_{1i}\mu_{2i} H_i \sqrt{P_{i-1}\rho_{i-1} - P_i \rho_i} \tag{44}$$

The term μ_{1i} is the flow coefficient for the ideal gas defined by Chaplygin [35], despite the fact that the real gas is considered in the model. The prediction error introduced by considering the real gas instead of the ideal gas in the thermodynamic process between the cavity and the orifice can be neglected, as reported in [36]. The term μ_{2i} is the energy carry-over coefficient introduced by Neumann [37]. This term considers the clearance perturbation, as suggested by Thorat and Childs [33]. The energy carry-over coefficient is equal to unity for the first cavity. The terms for the following cavities are obtained using:

$$\mu_{1i} = \frac{\pi}{\pi + 2 - 5 s_i + 2 s_i^2} \tag{45}$$

$$s_i = \left(\frac{P_{i-1}}{P_i}\right)^{\frac{\gamma - 1}{\gamma}} - 1 \tag{46}$$

$$\mu_{2i} = \sqrt{\frac{NT}{(1 - J_i)NT + J_i}} \tag{47}$$

$$J_i = 1 - \left(1 + 16.6\frac{H_i}{L_i}\right)^{-2} \tag{48}$$

When the flow sonic condition is reached under the last tooth (choked flow), the leakage mass flow-rate becomes independent by the downstream pressure [38]. To check if the flow is subsonic or choked, the axial velocity is compared with the speed of sound (ς) of the fluid. The speed of sound is evaluated using the NIST code [32] and it is function of the pressure and of the density of the previous cavity ($\varsigma_i = f(P_{i-1}, \rho_{i-1})$), whereas, the axial velocity is estimated using the definition of the leakage mass flow-rate, which is:

$$U_i = \frac{\dot{m}_i}{\mu_{1i} H_i \rho_{i-1}} \tag{49}$$

If the axial velocity is equal (*M*=1) or larger (*M*>1) than the speed of sound, the leakage mass-flow rate equation becomes:

$$\dot{m}_i = \mu_{1i} H_i \rho_{i-1} \varsigma_i \tag{50}$$

For the calculations of the shear stresses (τ_{si} for the seal and τ_{ri} for the rotor), it is necessary to use the correlation explicit formula to estimate the Fanning friction factor (f_{si} and f_{ri}). The shear stresses are evaluated using:

$$\tau_{si} = \frac{\rho_i}{2} f_{si} V_i^2 \operatorname{sgn}(V_i) \tag{51}$$

$$\tau_{ri} = \frac{\rho_i}{2} f_{ri} (R\Omega - V_i)^2 \operatorname{sgn}(R\Omega - V_i) \tag{52}$$

Several available models in the literature consider the Blasius correlation [14] on both the rotor and the stator wall for the friction factor. The Darcy friction factor correlation used by the authors is the one developed by Swamee and Jain [39], and the explicit formula is also valid for rough pipes, which is different from the Blasius correlation [40].

$$f_i = 0.25\left(\log_{10}\left(\frac{e/Dh_i}{3.7} + \frac{5.74}{Re^{0.9}}\right)\right)^{-2} \tag{52}$$

The continuity, circumferential momentum and energy zeroth-order equations were iteratively solved using the multi-variate Newton Raphson algorithm to find the solutions for the pressure, density, enthalpy and circumferential velocity for each cavity. The full details are reported in [41].

3.2. Labyrinth seal experimental tests and results

The experimental tests have been performed on the high-pressure seal test rig as it is described in [24].

The numerical results of the model described in the section 3.1 are now compared with the experimental results. The dynamic coefficients are calculated by using the energy equation or not (isenthalpic process).

The effects of the energy equation in the 1CV bulk-flow model for both positive and negative pre-swirl values are shown in Figure 10 - Figure 15. Figure 10 and Figure 11 show the numerical and experimental results for the direct stiffness coefficients versus the whirling speeds.

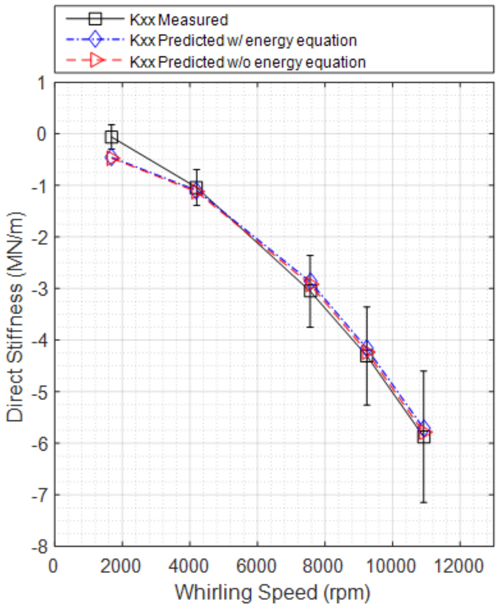

Figure 10 Direct stiffness coefficients: positive pre-swirl.

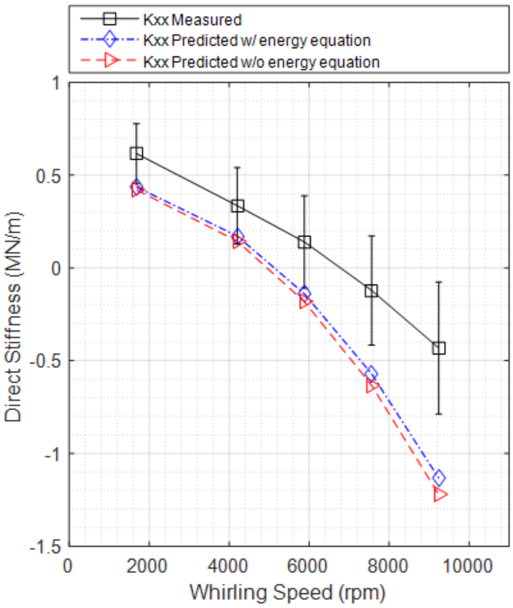

Figure 11 Direct stiffness coefficients: negative pre-swirl.

Figure 12 and Figure 13 show the numerical and experimental results for the cross-coupled stiffness coefficients. In the case of the negative pre-swirl ratio, the coefficients are negative, which implies that the effective damping (see Eq.(34)) is positive and justifies the wide system stability margin in the case of the negative pre-swirl (due to both the negative cross-coupled stiffness shown in Figure 13 and the positive direct damping shown in Figure 15). The direct damping coefficients versus whirling speeds are shown in Figure 14 and Figure 15. Figure 10 - Figure 15 show that the energy equation model is effective only on the cross coupled terms with the negative pre-swirl.

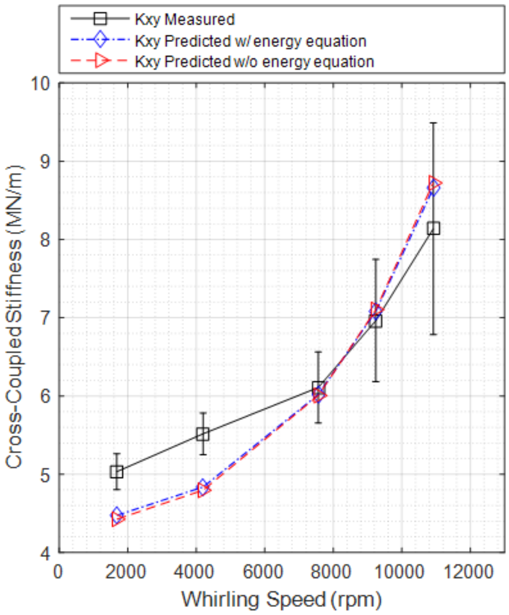

Figure 12 Cross-coupled stiffness coefficients: positive pre-swirl.

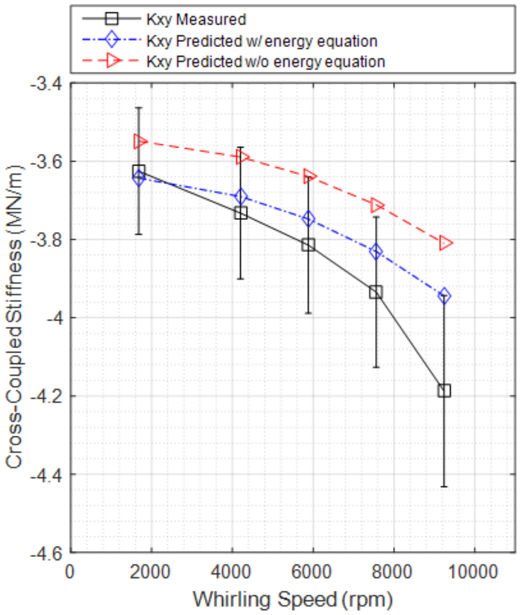

Figure 13 Cross-coupled stiffness coefficients: negative pre-swirl.

In the case of positive pre-swirl, the effect of the energy equation is negligible with respect to the results obtained using the isenthalpic model (see Figure 10, Figure 12 and Figure 14). On the contrary, in the case of negative pre-swirl, due to the higher fluid-rotor shear stress, the coupling between the continuity equation and the circumferential momentum equation can be observed. The effect of the energy equation can be noticed in the prediction of the cross-coupled stiffness coefficients (see Figure 13). The root cause is addressed to the changing of the steady pressure in the seal cavities (P_{0i}), see Figure 16, which influence the dynamic coefficients.

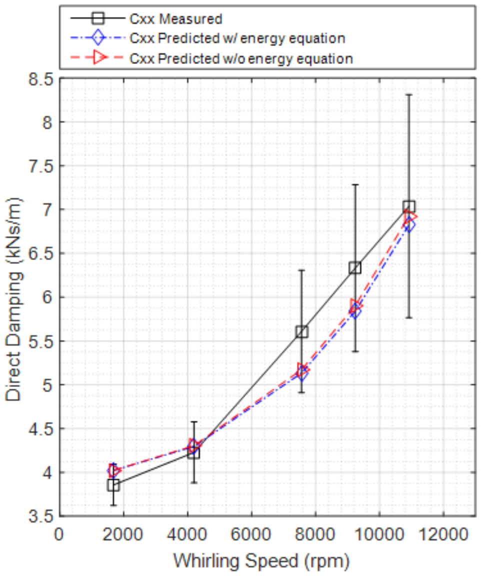

Figure 14 Direct damping coefficients: positive pre-swirl.

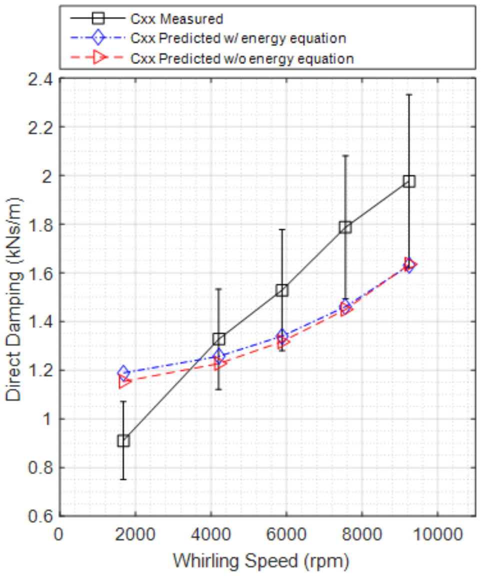

Figure 15 Direct damping coefficients: negative pre-swirl.

The effect of the enthalpy appears also in the first-order system of equations in the estimation of the *i*-th term $\partial\rho_i/\partial P_i|_{P_{0i},h_{0i}}$ that depends on the steady pressure and steady enthalpy.

6. Conclusions

The paper presented the models developed at the Dept. of Mechanical Engineering of Politecnico di Milano for the calculation of the dynamic effects of TPJB and labyrinth seals.

The results of the models have been validated by means of experimental tests performed on test-rig made on purpose.

In general, the results obtained present good fitting between the calculated parameters and the measured ones, therefore the proposed models can be profitably used in the design phase of rotating machines, allowing high performances/efficiencies to be reached.

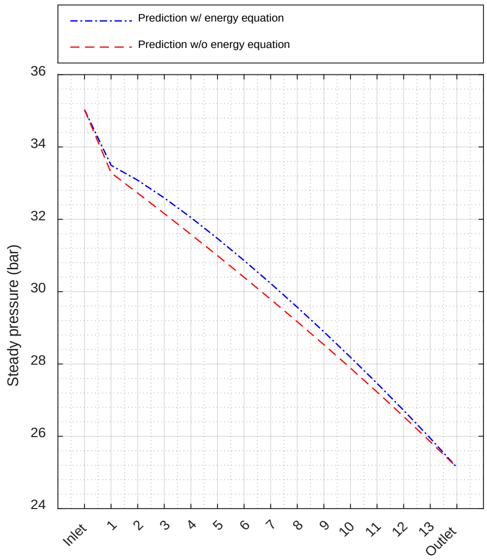

Figure 16 Steady pressure: negative pre-swirl.

References

[1] Lund JW. Spring and Damping Coefficients for Tilting Pad Journal Bearing. Transactions of the ASLE 1964;7:342-352. **(Periodical)**

[2] Yan Z, Wang L, Qiao G, Zheng T. An analytical model for complete dynamical coefficients of a tilting-pad journal bearing. Tribol Int 2010; 43:7-15. **(Periodical)**

[3] Qiuying C, Peiran Y, Yonggang M, Shizhu W. Thermoelastohydrodynamic analysis of the static performance of tilting-pad journal bearings with the Newton–Raphson method. Tribology International 2002;35(4):225-234. **(Periodical)**

[4] Dmochowski W, Dadouche A, Fillon M. Numerical study of the sensitivity of tilting-pad journal bearing performance characteristics to manufacturing tolerances: dynamic analysis. Tribology Trans 2008;51(5):573–580. **(Periodical)**

[5] Pennacchi P, Introduction of advanced technologies for steam turbine bearings. Advances in steam turbines for modern power plants. T. Tanuma ed. 2017, Woodhead Publishing – Elsevier. 321-360. **(Book)**

[6] Zhou H, Zhao S, Xu H, Zhu J. An experimental study on oil-film dynamic coefficients. Tribology International 2004;37(3):245–253. **(Periodical)**

[7] Varela AC, Nielsen BB, Santos IF. Steady state characteristics of a tilting pad journal bearing with controllable lubrication: Comparison between theoretical and experimental results. Tribology International 2013;58:85-97. **(Periodical)**

[8] Lihua Y, Huiguang L, Lie Y. Dynamic stiffness and damping coefficients of aerodynamic tilting-pad journal bearings. Tribology International 2007;40(9):1399-1410. **(Periodical)**

[9] Cha M, Glavatskih S. Nonlinear dynamic behaviour of

vertical and horizontal rotors in compliant liner tilting pad journal bearings: Some design considerations. Tribology International 2015;82, Part A:142-152. **(Periodical)**

[10] Simmons GF, Varela AC, Santos IF. Dynamic characteristics of polymer faced tilting pad journal bearings. Tribology International 2014;74:20-27. **(Periodical)**

[11] Delgado A, Vannini G, Ertas BM, Drexel M, Naldi L. Identification and Prediction of Force Coefficients in a Five-Pad and Four-Pad Tilting Pad Bearing for Load-on-Pad and Load-Between-Pad Configurations. J. Eng. Gas Turbines Power 2011; 133(9), 092503. **(Periodical)**

[12] Pennacchi P, Vania A, Chatterton S. Nonlinear Effects Caused by Coupling Misalignment in Rotors Equipped with Journal Bearings. Mechanical Systems and Signal Processing 2012;30:306-322. **(Periodical)**

[13] Jones GJ, Martin FA. Geometry Effects in Tilting-Pad Journal Bearings. Transactions of ASLE 1979;22(3):227-244. **(Periodical)**

[14] Childs D. Turbomachinery Rotordynamics - Phenomena, Modeling, and Analysis. New York: John Wiley & Sons, 1993. **(Book)**

[15] Vance J, Zeidan F, Murphy B, Machinery Vibration and Rotordynamics. John Wiley & Sons, 2010. **(Book)**

[16] Bachschmid N, Pennacchi P, Vania A. Steam-whirl analysis in a high pressure cylinder of a turbo generator. Mechanical Systems and Signal Processing, 2008;22(1): 121-132. **(Periodical)**

[17] Childs DW, Scharrer JK. An Iwatsubo-Based Solution for Labyrinth Seals: Comparison to Experimental Results. Journal of Engineering for Gas Turbines and Power, 1986;108:325-331. **(Periodical)**

[18] Iwatsubo T. Evaluation of Instability Forces of Labyrinth Seals in Turbines or Compressors. NASA CP 2133, Proceedings of a Workshop at Texas A&M University, Rotordynamic Instability Problems in High Performance Turbomachinery.1980:205-222. **(Proceedings)**

[19] Scharrer J. Theory versus experiment for the rotordynamic coefficients of labyrinth gas seals: part I - A two control volume model. Journal of Vibration, Acoustics, Stress, and Reliability in Design. 1988;110(3):270-280. **(Periodical)**

[20] Wyssmann H, Pham T, Jenny R. Prediction of Stiffness and Damping Coefficients for Centrifugal Compressor Labyrinth Seals. ASME Journal of Engineering for Gas Turbines and Power vol. B. 1984;106:920-926. **(Periodical)**

[21] Nordmann R,. Weiser P. Evaluation of Rotordynamic Coefficients of Look-Through Labyrinths By Means of a Three Volume Bulk Flow Model. Rotordynamic Instability Problems in High-Performance Turbomachinery, NASA, CP-3122, 1991. **(Proceedings)**

[22] Childs D, Scharrer J. Theory Versus Experiment for the Rotordynamic Coefficient of Labyrinth Gas Seals: Part II - A Comparison to Experiment. Journal of Vibration, Acoustics, Stress, and Reliability in Design. 1988;110:281-287. **(Periodical)**

[23] Picardo A, Childs D. Rotordynamic Coefficients for a Tooth-on-Stator Labyrinth Seal at 70 Bar Supply Pressures: Measurements Versus Theory and Comparisons to a Hole-Pattern Stator Seal. Journal of Engineering for Gas Turbines and Power. 2004;127(4). **(Periodical)**

[24] Vannini G, Cioncolini S, Calicchio V, Tedone F. Development of a High Pressure Test Rig for Cemtrifugal Compressors Internal Seals Characterization. Proceedings of the Fortieth Turbomachinery Symposium, Vols. Houston, Texas , September 12-15, 2011. **(Proceedings)**

[25] Wilkes JC, Childs DW. Tilting Pad Journal Bearing - A Discussion on Stability Calculation, Frequency Dependence, and Pad and Pivot. J. Eng. Gas Turbines Power 2012;134(12), 122508. **(Periodical)**

[26] Hori Y. Hydrodynamic Lubrication. 1st ed. Verlag Tokyo: Springer; 2006. **(Book)**

[27] Stachowiak GW, Batchelor AW. - Engineering Tribology, Butterworth-Heinemann, 2011. **(Book)**

[28] Kirk RG, and Reedy SW. Evaluation of Pivot Stiffness for Typical Tilting-Pad Journal Bearing Designs. J. Vib., Acoustics, Stress, and Reliability in Design, 1988; 110:165-171. **(Periodical)**

[29] Dang, PV, Chatterton S, Pennacchi P. Effect of the load direction on non-nominal five-pad tilting-pad journal bearings. Tribology International 2016;98:197-211. **(Periodical)**

[30] Rouvas C, Childs D. A Parameter Identification Method for the Rotordynamic Coefficients of a High Renoylds Number Hydrostatic Bearing. J. Vib. Acoust 1993;115(3):264-270. **(Periodical)**

[31] Ricci R, Chatterton S, Pennacchi P. Robust estimation of excitation in mechanical systems under model uncertainties. Journal of Sound and Vibration, 2013;332(2):264–281. **(Periodical)**

[32] Huber M. NIST thermophysical properties of hydrocarbon mixture database (SUPERTRAPP), Version 3.1,U.S. Department of Commerce, National Institute of Standards and Technology. Gaithersburg, MD, 2003. **(Computer software)**

[33] Thorat M and Childs D. Predicted Rotordynamic Behavior of a Labyrinth Seal as Rotor Surface Speed Approaches Mach 1. Journal of Engineering for Gas Turbines and Power. 2010;132(11):8. **(Periodical)**

[34] White F. Fluid Mechanics. McGraw Hill, 7th Edition, 2009. **(Book)**

[35] Gurevich M. The theory of jets in an ideal fluid. Pergamon Press, Oxford, 1966:319-323. **(Book)**

[36] Wang W, Yingzheng L, Puning J. Numerical investigation on influence of real gas properties on nonlinear behavior of labyrinth seal-rotor system. Applied Mathematics and Computation 2015;263:12-24. **(Periodical)**

[37] Neumann K. Zur Frage der Verwendung von Durchblicktungen im Dampgturbinebau. Maschinentechnik 1964;13(4). **(Periodical)**

[38] Gamal A. Leakage and Rotordynamic effects of Pocket Damper Seals and See-Through Labyrinth Seals. Ph.D Dissertation, Texas A&M University, 2007. **(Thesis)**

[39] Swamee P, Jain A. Explicit equations for pipe-flow problems. Journal of the Hydraulics Division-American Society Civil Engineers. 1976;102(5): 657-664. **(Periodical)**

[40] Kiijarvi J. Darcy friction factor formulae in turbulent pipe flow. Lunowa Fluid Mechanics. Paper, no. 110727, 2011. **(Periodical)**

[41] Cangioli F, Pennacchi P, Vannini G, Ciuchicchi L. Effect of energy equation in one control-volume bulk-flow model for the prediction of labyrinth seal dynamic coefficients. Mechanical Systems and Signal Processing. 2018;98:594-612. **(Periodical)**